

Mechanical and metallurgical properties of GTAW dissimilar welds between SUS304 and SA213T11 using ER308 filler metal, preliminary study

Hamdani^{1,2}, Akhyar^{1,3*} , Thaib Rizwan⁴, Agus Sasmito⁵, H Agus Suhartono⁶

¹ Doctoral Program-School of Engineering, Universitas Syiah Kuala, Jl. Tgk. Chik Pante Kulu No. 5 Komplek Universitas Syiah Kuala, Banda Aceh 23111, Indonesia

² Department of Mechanical Engineering, Politeknik Negeri Lhokseumawe, Jl. Banda Aceh-Medan KM. 280 Buketrata, Lhokseumawe 24301, Indonesia

³ Department of Mechanical Engineering, Universitas Syiah Kuala, Jl. Syech Abdurrauf No.7 Darussalam, Banda Aceh 23111, Indonesia

⁴ Department of Capture Fisheries, Marine and Fisheries Faculty, Universitas Syiah Kuala, Jl. Putro Phang, Darussalam, Banda Aceh 23111, Indonesia

⁵ National Research and Innovation Agency of Indonesia, Jl. Hidrodinamika, Sukolilo, Surabaya 60112, Indonesia

⁶ National Research and Innovation Agency of Indonesia, Jl. Raya Puspitek Kawasan Sains dan Teknologi KST BJ. Habibie, Serpong, Gedung 220, Setu, Tangerang Selatan 15314, Indonesia

* Corresponding author's e-mail: akhyar@usk.ac.id

ABSTRACT

Dissimilar welding between austenitic stainless steel SUS304 and low alloy ferritic steel SA213T11 is widely used in the petrochemical and power generation industries because this combination is suitable for use in corrosive and high-temperature environments. This study presents a preliminary investigation of dissimilar metal welding between austenitic stainless steel SUS304 and low-alloy steel SA213T11 using gas tungsten arc welding (GTAW) with ER308 filler metal. The mechanical and metallurgical properties of the welded joints were evaluated through hardness testing, tensile testing, bend testing, and microstructural analysis. The results show that the welds produced are of acceptable quality, with sound bead appearance and no visible surface defects. Hardness values vary across different weld regions, with the weld zone exhibiting higher hardness due to the presence of δ -ferrite. Tensile tests indicate that the weld strength is comparable to or greater than the weaker base metal, and failure occurs outside the weld region. Microstructural observations reveal significant changes in the heat-affected zones and weld metal, influenced by the thermal cycle and filler composition. These findings provide insight into the performance of ER308 in joining dissimilar metals, which is relevant for applications in power and petrochemical industries.

Keywords: dissimilar welding, GTAW, SUS304, SA213T11, ER308, mechanical properties, microstructure.

INTRODUCTION

Stainless Steel is widely used as a superheater steam pipe in the petrochemical industry and power generation due to its corrosion resistance, strength, and resistance to high temperatures and extreme environments [1–6]. Low-carbon austenitic grades are chosen for welding that

will be used in corrosive environments because they limit the occurrence of carbide precipitation. Type 304, which has a maximum carbon content of 0.08%, is commonly used [7]. For reasons of efficiency, in its application, SUS304 is welded with other materials that are suitable for working conditions such as low alloy steel, for example, SA213T11, which has good mechanical properties,

high corrosion and oxidation resistance, and is ideal for high temperatures [8].

The joining of two different materials by welding is a dissimilar welding process [9]. This dissimilar combination is often required in critical components such as heat exchangers, superheaters, and piping systems in power plants and petrochemical industries, where there is a need to transition between corrosion-resistant and high-temperature-resistant materials. The ability to reliably join these two materials is essential for improving system performance and reducing maintenance costs.

During the welding cycle, local heating causes the temperature distribution in the component to be non-uniform and changes as the welding progresses. Differences in mechanical properties, chemical composition, and metallurgical structure can produce different material characteristics between the weld metal (WM), heat affected zone (HAZ), and base metal (BM) [10–12]. Gas tungsten arc welding (GTAW) is widely used for dissimilar welding because of its accuracy and ability to produce high-quality welds. Almost every type of metal can be welded with GTAW, and the heat input can be easily controlled [13–15]

Choosing the right filler metal for dissimilar welding is challenging because it must closely match the base metal's alloy [16]. In welding between austenitic stainless steel type 304 and low alloy ferritic steel type SA213T11, the use of austenitic-based filler metal is certainly suitable for stainless steel because it has the same thermal properties [17]. Austenitic base filler metal ER308 is ideal for welding stainless steel type 304 because of its suitable thermal expansion coefficient, but its compatibility with SA213T11 low alloy ferritic steel needs to be considered. Selection of appropriate filler metal to ensure sufficient alloying in dilution low alloy steel [18–20]. When welding austenitic stainless steel to low alloy ferritic steel, the dilution effect of the base metal on the weld metal is crucial. Therefore, careful selection of filler metal and planning of the welding procedure are essential to maintain a small but vital amount of delta ferrite [21–24]. Delta ferrite is needed to prevent hot cracking [25, 26].

Previous studies on dissimilar welding between austenitic stainless steel and low alloy ferritic steel using certain filler metals have been conducted. Among them are weldings between SA312 type 304LN austenitic stainless steel with

SA508 Gr.3 Cl.I ferritic steel, using filler metal IN 82 [27], SUS304 austenitic stainless steel with ASTM A335 P92 ferritic steel, using nickel-based Alloy 82 filler metal (AWS A5.14 ERNiCr-3) [28], stainless steel grade SS 304 with medium carbon steel EN 8, using filler metal ER 309 L [29], AISI 304L austenitic stainless steel with AISI 1005 low carbon ferritic steel, using filler metal ER309L [30], austenitic stainless steel TP347H with low alloy ferritic steel G102, using nickel-based filler metal [31], AISI304L with API5LX65, using filler metal metal composites ER309L, ERNiCr3, and ER308L [32], SUS 304 with SUS316, using C-Mn filler metal [33], Friction rotary welding (FRW), electron beam welding (EBW), and GTAW are used to create AISI 304 and AISI 4140 dissimilar joints [34], low alloy steel API X70 with UNS S31803, using ER2209 filler metal [35].

Various welding methods have been tested for joining different metals. Friction stir welding (FSW) is known for making strong and clean joints, especially when joining aluminium to copper or steel. It also reduces the area affected by heat and makes the joint stronger [36]. MAG welding is commonly used in industries to join various types of steel. The combined plasma and MAG welding method can also be used for joining metals [37]. Researchers study different metal pairs, like stainless steel with carbon steel, Inconel with low alloy steels, and aluminium with copper, to solve problems like metal incompatibility and brittle compounds. These studies show that welding different metals is complicated and choosing the right welding method is important to get the best joint quality.

ER308 is commonly used for joining austenitic stainless steels and offers good weldability and corrosion resistance. However, ER309L containing higher chromium and nickel offers improved compatibility with ferritic steels and better resistance to hot cracking. In more demanding applications, Ni-based fillers such as Inconel 82 provide excellent metallurgical compatibility and superior corrosion resistance, especially at high temperatures [18, 38].

There are no previous studies using ER308 between SUS304 and SA213T11. This research aims to characterize the results of dissimilar welding with metallurgical testing and mechanical testing, such as tensile testing, bending testing, and hardness testing. Comparison with the base metal is the main focus in relation to the mechanical properties of the weld. The goal is to ensure that the weld structure is not the weakest

part. These findings will provide baseline data for further optimization of welding parameters and contribute to a better understanding of the performance of these joints in service.

MATERIALS AND METHODS

Materials

Austenitic stainless steel grade SUS304 and low alloy ferritic steel SA213T11 with a pipe outer diameter of 44.5 mm and thickness of 4 mm. Filler metal ER308 with a diameter of 2.4 mm was used in this study. The chemical composition and mechanical properties of the base metal and filler metal are shown in Table 1 and Table 2

Welding using austenitic filler metal generally produces a weld metal composition of 4–12% delta ferrite [16, 39]. The Schaeffler diagram is used to estimate the phase, composition, and microstructure of the weld deposit [40, 41]. In GTAW welding, the weld metal composition consists of a dilution of the base metal of 20-50% [9, 42–44]. Assuming the dilution of the GTAW welding process, each base metal is 30%, where each base metal is diluted with the same composition and the ER308 filler metal is 70%, according to the chemical composition of the base metal and filler metal in Table 1, the Schaeffler diagram for dissimilar welding between SUS304 and SA213T11 is shown in Figure 1.

Methods

GTAW welding with DCEN current was used to make dissimilar welds. V-groove butt joint and multi-pass welding with 70° bevel angle

and 1 mm root (Figure 2a). Welding groove was machined by lathe (Figure 2b). Purging gas was inserted into the pipe to protect the root of the weld (Figure 2c). Purging gas (99.99% argon) is required in high-quality stainless steel welding to avoid oxidation in the weld area [45–47]. The welding parameters used, as shown in Table 3, were based on past studies and refined through preliminary tests to ensure strong, defect-free welds with a consistent bead shape. A current of 70–75 A and 18 V maintained a stable arc without damaging the thin SA213T11 pipe. The interpass temperature was kept at 200 °C to control the heat cycle and prevent the formation of hard phases in the affected area, especially on the SA213T11 side [48]. A welding speed of 3.0 mm/s provided a good balance between penetration and heat input [49]. Welding was performed in the fixed horizontal 5G position to simulate real conditions in power and petrochemical industries. Before dissimilar welding, the base metal SUS304 and SA213T11 were first tested for chemical composition by Optical Emission Spectrometry, referring to ASTM-E1086-22 standards for austenitic stainless steel and ASTM E415-21 for carbon and low alloy steel. The microstructure was observed by metallurgical microscope. The base metal is also tested for hardness using the micro Vickers hardness tester, in accordance with the JIS Z 2244-2020 standard, tensile testing using a universal testing machine, in accordance with the ASTM E8 standard. The results of welding dissimilar metal joints are tested for hardness using the micro Vickers method, microstructure observation, tensile testing according to the ASME Section IX standard, and U root bending testing according to the ISO 5173 standard.

Table 1. Chemical composition of base metal and filler metal as per ASTM standard [1, 8, 16]

Weight	C	Mn	Si	Cr	Ni	Mo	S	P	Cu
SUS304	0.08	2.00	1.00	18 - 20	8–10.5	-	0.03	0.045	-
SA213T11	0.05–0.15	0.3–0.6	0.5–1.00	1–1.5	-	0.44–0.65	0.025 max	0.025 max	-
ER308	0.03	1–2.5	0.3–0.65	19.5–22	9–11	0.75 max	0.03 max	0.03 max	0.75 max

Table 2. Mechanical properties of base metal and filler metal as per ASTM standard [1, 8, 16]

Mechanical properties	Min. yield strength (MPa)	Min. tensile strength (MPa)	Elastic modulus (GPa)	Hardness rockwell
SUS304	290	579	200	B80
SA213T11	205	415	215	B85
ER308	400	580	200	B89

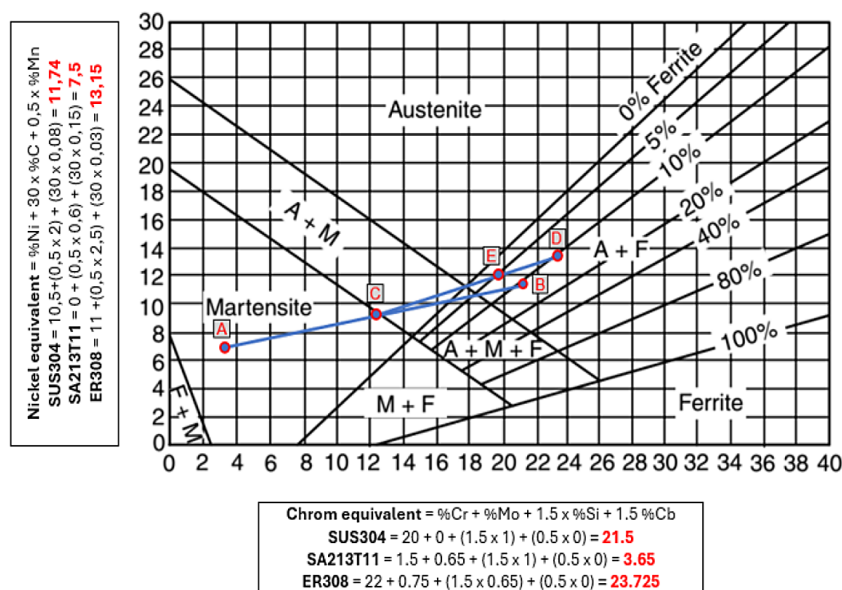


Figure 1. Schaeffler diagram for dissimilar welding (A) chromium and nickel composition coordinates for SA213T11, (B) chromium and nickel composition coordinates for SUS304, (C) midpoint between point A and point B (D) chromium and nickel composition coordinates for ER308, and (E) midpoint between point C and point D 30% base metal dilution

RESULTS AND DISCUSSION

Chemical composition and microstructure of base metal

The proposed base metal underwent a series of tests to ensure the performance and reliability of the welded joints. These tests help evaluate the metallurgical and mechanical properties of the base metal, providing information on its strength, durability, and potential failure mechanisms. The results of the chemical composition and microstructure tests of the base metal are shown in Table 4 and Figure 3. The results of the chemical composition tests indicate that the base metal has a suitable elemental composition and does not contain any undesirable elements that can affect the weld quality.

The results of the microstructure tests show an austenitic structure with a typical equal-axial grain pattern and no delta ferrite phase or carbide precipitates, indicating a stable primary structure under normal conditions. The microstructure is suitable for SUS304 material which is rich in chromium and nickel (Figure 3a). The microstructure of the SA213T11 material has a typical ferritic-pearlitic microstructure, which can be seen as ferrite grains with clear grain boundaries and pearlite scattered in it (Figure 3b).

Mechanical properties of base metal

Hardness testing was performed to identify potential hardness mismatches that could lead to stress concentration and cracking. The results of hardness testing at multiple points showed an average hardness of the base metal of 145 HV for SUS304 and 130 HV for SA213T11. Tensile testing provides important data on the overall strength and ductility of the weld, ensuring that the joint can withstand the applied load without premature failure. The base metal complies with the ASTM E8 standard tensile test sample (Figure 4a) and the base metal after tensile testing (Figure 4b). From the figure, it can be seen that SUS304 has a large strain before fracture compared to SA213T11, reflecting its highly ductile nature.

The curve of SUS304 has a longer elastic zone than SA213T11, followed by a wider plastic deformation before failure. The average maximum tensile strength is 579 MPa for SUS304 (Figure 5a). The curve shows that SA213T11 is more brittle than SUS304. The average maximum tensile strength is 569 MPa for SA213T11 (Figure 5b), which means it is more susceptible to failure due to high stress or thermal shock. Both figures show elastic and plastic zones before failure, although with different characteristics. Both base metal materials meet the tensile strength requirements of ASTM as Table 2.

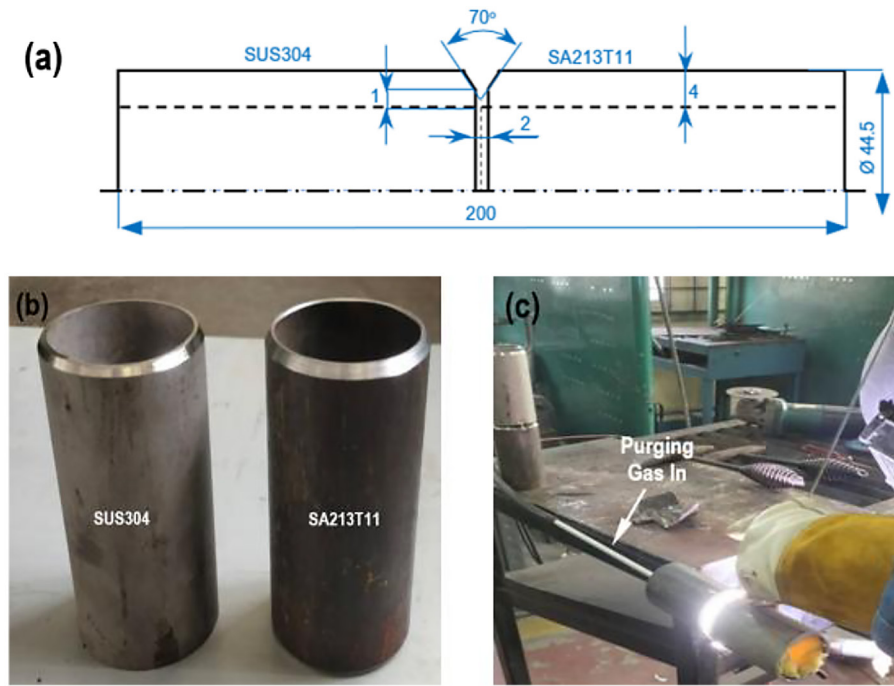


Figure 2. Dissimilar welding design (a) weld joint design, (b) weld groove, (c) purging gas filling

Table 3. Welding parameters used in the experiment

Parameter	Unit	Value
Power source	-	DCEN
Current	A	70–75
Voltage	V	18
Interpass temperature	°C	200
No. of welding passes	-	3
Welding speed	mm/sec	3.0
Electrode diameter	mm	2.4
Filler rod diameter	mm	2.4
Shielding gas	-	Argon
Purging gas	-	99.99% Argon
Gas flow rate	L/min	14
Welding position	-	5G horizontal fixed

Dissimilar welding results

Figure 6 shows the dissimilar GTAW welding of SUS304 and SA213T11 using ER308 filler metal. With currents of 70 A for root passes and 75 A for filling passes, the weld joint is of good quality, with a uniform surface and no visible defects.

Weld microstructure

The microstructure around the weld metal is very important to understand the metallurgical

bond between dissimilar materials, which can affect the properties of the joint. The macrostructure of a weld joint is shown in Figure 7a. In this image, the color and texture differences between the base metal and the weld metal are clearly visible, reflecting the characteristics of each material after the welding process. Figure 7b is a SEM image of a dissimilar weld joint showing the weld metal area in more detail.

The microstructure in Figure 8a shows the overall weld metal (WM), fusion zone (FZ), and boundary between SA213T11 base metal and ER308 weld metal. The microstructural differences between the two materials are clearly visible, reflecting the characteristics of each material and the influence of the melting and cooling processes during welding. Figure 8b is an enlargement of the area near the fusion line. The HAZ area of SA213T11 is visible, indicating microstructural changes due to thermal cycling during welding. The fusion line separating the HAZ and weld metal is characterized by changes in grain morphology. In addition, the presence of δ -ferrite in the ER308 weld metal is clearly visible, which plays a role in increasing resistance to hot cracking during solidification. Various zones formed by the welding process, including the fusion boundary, HAZ, and austenite grains are visible in Figure 8c. The ER308 weld metal shows a typical solidification structure, which generally contains

Table 4. OES analysis results of base metal chemical composition

Sample	Chemical composition (weight %)													Material
	C	Si	S	P	Mn	Ni	Cr	Mo	V	Cu	Sn	Al	Fe	
No. 1	0.0320	0.7209	0.0028	0.0366	1.4934	8.2533	17.2930	0.1044	0.0533	0.2867	0.0111	0.0158	71.6967	Stainless steel
No. 2	0.0754	0.6538	0.0018	0.0043	0.4576	0.0098	0.9538	0.4847	0.0094	0.0141	0.0003	0.0119	97.3195	Low alloy steel

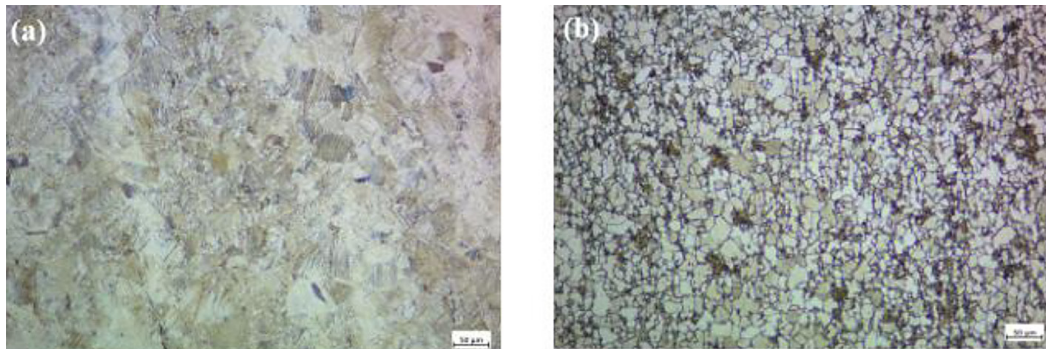


Figure 3. Base metal microstructure, (a) SUS304, etched with 10% Nital for 24 h, (b) SA213T11, etched with 3% Nital for 10 s

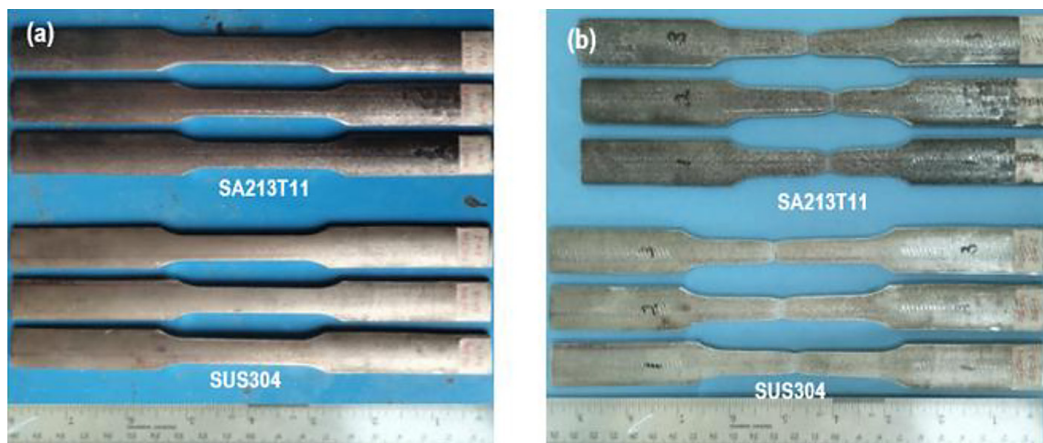


Figure 4. Base metal tensile test samples, (a) ASTM E8 standard tensile test samples, (b) base metal candidates after tensile testing

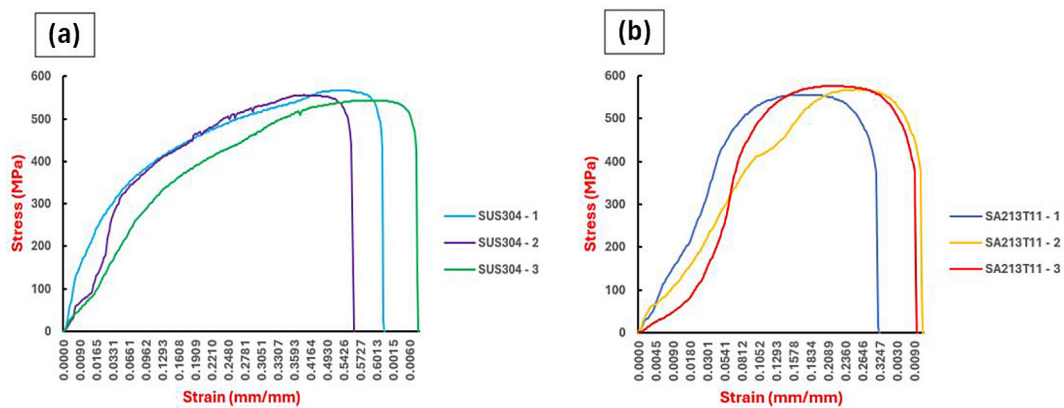


Figure 5. Stress-strain diagram of base metal, (a) stress-strain diagram of SUS304, (b) stress-strain diagram of SA213T11

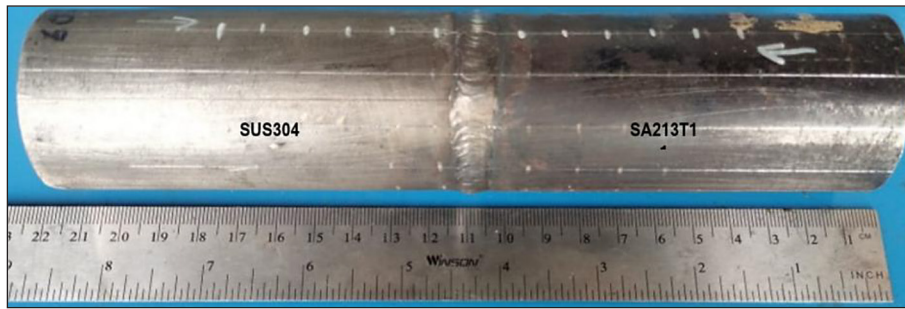


Figure 6. Dissimilar welding results between SUS304 and SA213T11

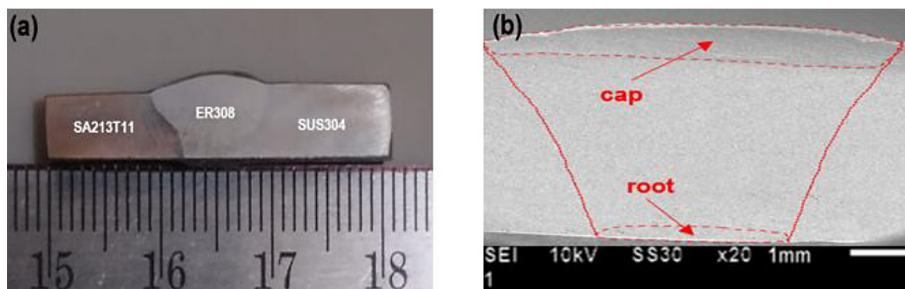


Figure 7. Macrostructure of dissimilar welded joints (a) and (b) SEM images

a mixture of austenite phases with δ -ferrite to improve resistance to hot cracking. On the right side, SUS304 shows more defined austenite grains with different sizes and orientations. The fusion boundary is marked by a dashed line indicating the transition between ER308 and SUS304. Right next to this boundary, the HAZ region experiences microstructural changes due to the welding thermal cycle.

In Figure 8d the typical austenitic structure is clearly visible, with a grain pattern sandwiched by grain boundaries and the presence of interdendritic structures. Figure d. has a microstructure dominated by the austenite phase with high ductility and good corrosion resistance. The solidification structure consisting of austenite grains with a dark interdendritic network is seen in Figure 8(e). The distribution of δ -ferrite is net-like or branched among the austenite grains originating from the weld metal [50]. Delta ferrite forms during the solidification of austenitic stainless steels due to the chemical composition and solidification mode. Small amount (~5–10%) can improve resistance to solidification cracking and enhance corrosion resistance, which are critical for weld quality and durability.

The microstructure dominated by ferrite phase with pearlite distribution spread throughout the matrix is shown in Figure 8(f). Pearlite, which

consists of layers of ferrite and cementite (Fe_3C), plays a role in increasing the strength and wear resistance of the material.

Microhardness of welds

Figure 9 shows the distribution of hardness values along the weld zone, starting from the BM, HAZ, to the WZ on three specimens. The average hardness on the BM of SUS304 is 133 HV, on the HAZ side of SUS304 is 137 HV. In contrast, the HAZ on the SA213T11 side shows a relatively small change in hardness, where the average hardness is 129 HV, which is slightly different from the average hardness of the SA213T11 base metal of 127 HV. This increase is due to microstructural changes due to the welding thermal cycle, such as the formation of partial martensite or the solidification of ferrite and pearlite phases. It can be seen that the average hardness value in the WZ zone has the highest value compared to other areas, which is 153 HV. This can be attributed to the presence of a δ -ferrite structure in the ER308 weld metal which increases the hardness due to rapid cooling after welding. Different hardness values in dissimilar welded joints indicate that other mechanical properties also have different characteristics, and if the difference is significant, it can cause the

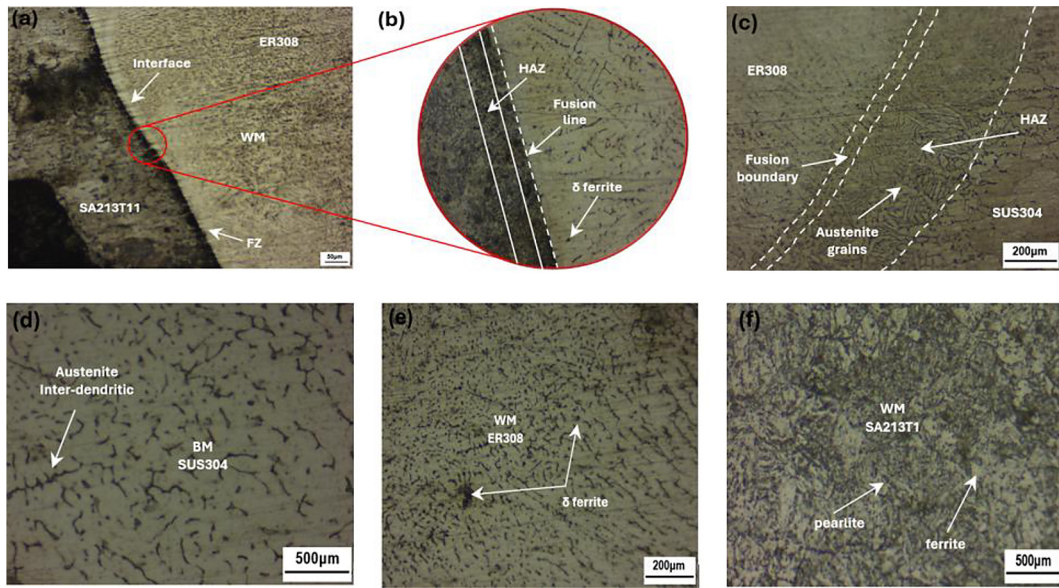


Figure 8. Microstructure of welded joints, etched with HCL + HNO₃ for 10 seconds (a) area between WM and SA213T11 (b) enlargement of image a (c) area between WM and SUS304 (d) BM SUS304 (e) WM ER308, (f) BM SA213T11

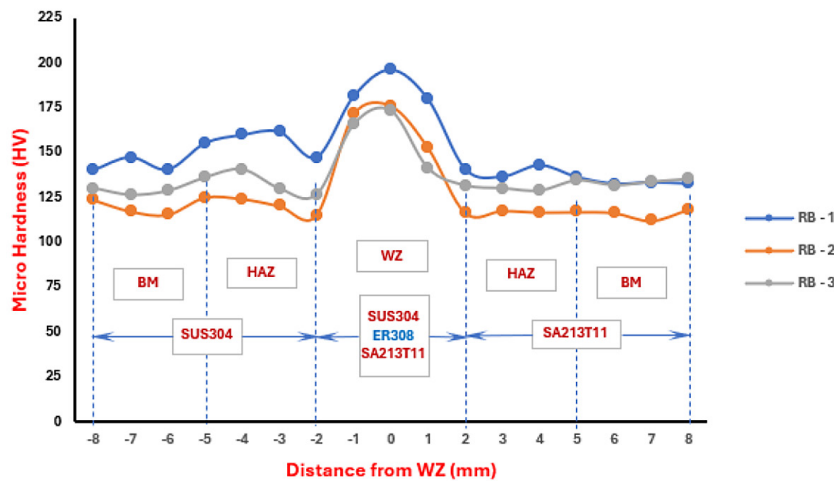


Figure 9. Hardness distribution in dissimilar welded joints

dissimilar weld joint to be more susceptible to fatigue or dynamic loads [51–53].

In practical applications, such as in pressure vessels, heat exchangers, or piping systems, these variations in hardness across different weld zones can significantly affect service performance. Higher hardness improves wear resistance, but mismatches can create stress points, raising fatigue failure under cyclic loading. Additionally, minor process issues, such as arc fluctuation and manual welding inconsistencies, can lead to localized hardness variations and microstructural shifts, particularly in HAZ. These challenges are common in manual GTAW and

are well-documented in studies on dissimilar metal welding.

Tensile strength of weld

Figure 10 shows the tensile test results on dissimilar welded joints. In Figure 10a, three tensile test specimens are shown after testing, showing the location and pattern of fracture that occurred. It can be seen that the fracture occurred at the same location, namely in the SA213T11 base metal, which showed lower mechanical characteristics of the material than the SUS304 base metal and ER308 weld metal. It can be seen that none of

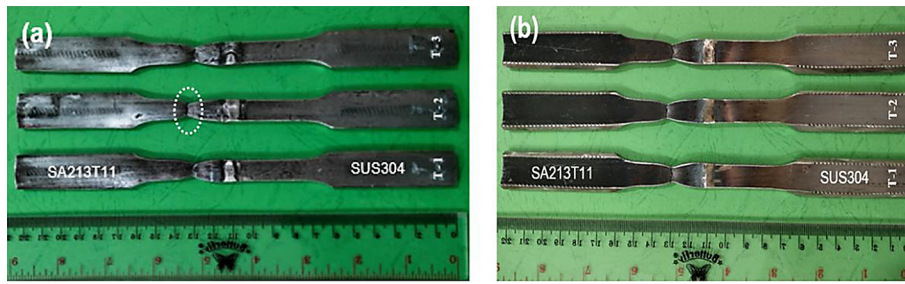


Figure 10. Tensile testing of dissimilar welds (a) sample after breaking (b) sample after breaking in reverse position

the samples broke in the weld area, indicating that the welding design and parameters used have met the required strength criteria. The same specimen but in an inverted position is shown in Figure 10(b). The inside of the SA213T11 material looks darker in color compared to SUS304. This is due to the production process involving high heating, such as normalizing or annealing heat treatment. This process can cause the formation of an oxide layer on the inner surface of the pipe, especially if pickling or chemical cleaning is not carried out after production.

Figure 11 shows that the weld-1 specimen (yellow) has a lower tensile strength than the weld-2 specimen (red) but higher than the weld-3 specimen (blue), also has a fairly high strain, but lower than the weld-2 specimen. The highest maximum stress in the weld-2 specimen is 520 MPa, this specimen also has the highest strain before fracture, indicating a more ductile nature. The weld-3 specimen has the lowest maximum stress of 412 MPa, indicating that this weld joint is weaker than the other two specimens and also

has the smallest strain, indicating that this specimen is more brittle than the other two. The shape of the curve shows that the average maximum stress is 461 MPa. All specimens experience plastic deformation before fracture, but the degree of deformation varies.

Bending strength of welds

There are three welding specimens labeled RB-1, RB-2, and RB-3 (Figure 12a). All specimens show welding results with a clear fusion zone in the center of the joint. In Figure 8b, specimens RB-2 and RB-3 appear to have indications of cracking in the root weld area. RB-1 shows more uniform results with no indication of large cracks, but still has a lighter area, possibly due to incomplete penetration. RB-2 and RB-3 show cracking due to the influence of force during testing, indicating possible weaknesses in the joint or suboptimal mechanical properties of the weld.

Figure 13 shows that Bend-1 has the highest maximum stress at 2433 MPa, meaning it can

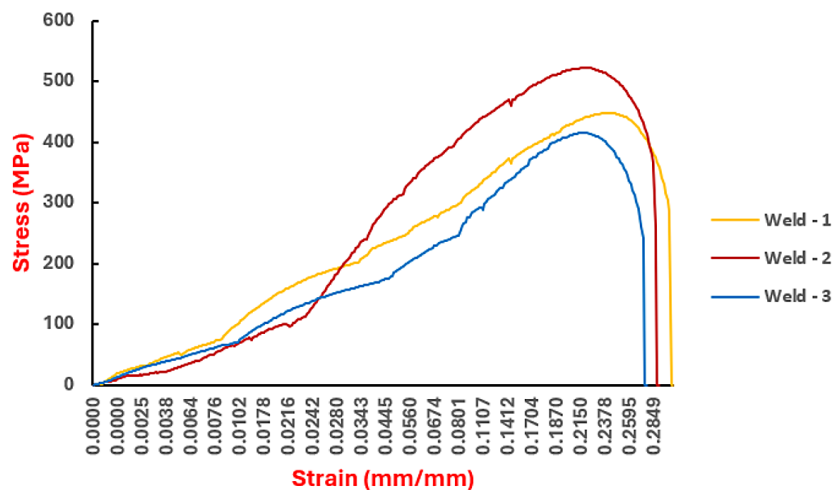


Figure 11. Dissimilar welded joint stress and strain graph

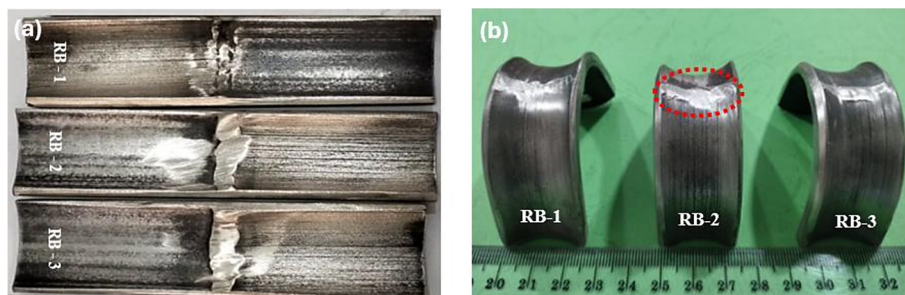


Figure 12. Root U-bend tests of dissimilar joints (a) U-bend test specimens (b) test results

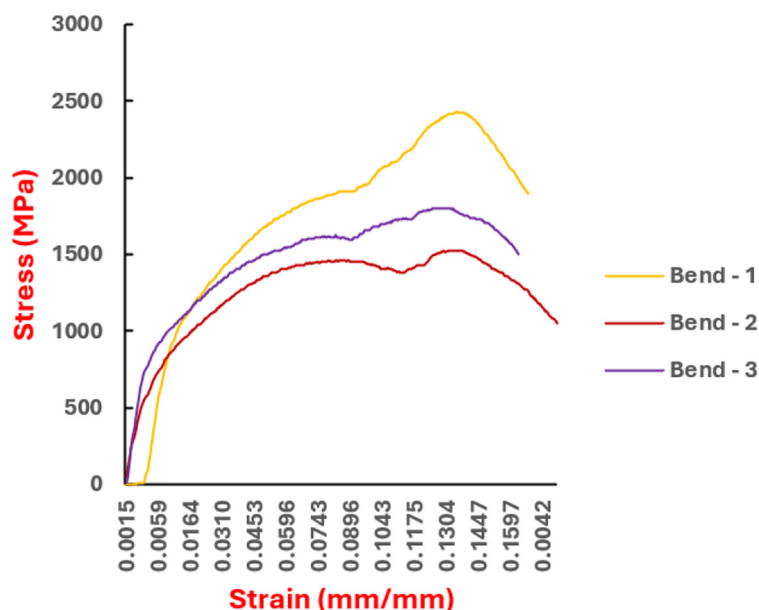


Figure 13. Stress and strain graph of U root bending test of dissimilar welded joints

handle more bending stress before failing. Bend-2 has the lowest at 1520 MPa, making it more prone to failure. Bend-3, with 1805 MPa, falls between Bend-1 and Bend-2 in strength.

CONCLUSIONS

The average hardness of the base metal is 145 HV for SUS304 and 130 HV for SA213T11, while the average maximum tensile strength is 559 MPa for SUS304 and 569 MPa for SA213T11. The highest hardness is found in the weld zone (153 HV) due to the presence of δ -ferrite, while the hardness in BM SUS304, HAZ SUS304, BM SA213T11, and HAZ SA213T11 ranges from 127–136 HV. This variation in hardness reflects the difference in mechanical properties in dissimilar welded joints due to microstructural changes during welding.

The tensile test shows that the base metal SA213T11 fractures, meaning it is weaker than SUS304 and weld metal ER308. Since there are no fractures in the weld area, the welding meets strength standards, with a maximum stress of 461 MPa.

The base metal has an appropriate elemental composition. SUS304 has an austenitic structure with uniform grains, while SA213T11 has a ferritic-pearlitic structure with scattered ferrite and pearlite grains. The FZ and HAZ change due to welding heat. Filler metal ER308 forms austenite and δ -ferrite, improving resistance to hot cracking and corrosion. SUS304's austenite grains vary, while SA213T11's ferritic-pearlitic structure enhances strength and wear resistance.

This research has a significant impact on the industrial world, especially in the fields of manufacturing, energy, and construction. The studies suggest that ER308 can be safely used in

high-temperature applications with SA213T11. For future research, several areas can be explored to be further improved and not limited to the application of welding current variations to observe their effects on the mechanical and metallurgical properties of different welded joints. Using more sophisticated techniques in phase analysis, such as SEM or EDS. Using residual stress measurement using X-ray diffraction (XRD) to be able to evaluate its effect on weld performance. Application of computational and simulation approaches using Finite Element Analysis which includes thermal cycle models, stress distribution, and distortion to optimize welding parameters.

Acknowledgments

This publication was made possible by a grant from the Research Fund of the Ministry of Research, Technology, and Education, Republic of Indonesia.

REFERENCES

- Committee of Stainless Steel Producers. The Role Stainless Steel in Industrial Heat Exchangers. *Stainl. Steel Ind. Data*. 2006; 8. Available from: https://www.nickelinstitute.org/~media/Files/Technical-Literature/RoleofStainlessSteelsinIndustrialHeat-Exchangers_9005.ashx
- Agreement L, Material W. Inherently Reliable Boiler. *Manager*. 2006; 3(3).
- Chandrasekaran K., Kumar P. R., Ramanathan R., Chandradass J., Kannan T. T. M., and Rajan A. J. Characteristic analysis of dissimilar metal weld for AISI304 with SA213T22 in super heater coils, *Mater. Today Proc.*, 2021; 45, 6788–6793. <https://doi:10.1016/j.matpr.2020.12.671>
- Arivarasan J. and Kannan T. D. B. Mechanical and metallurgical characterisation of double pulse mig welded in 617-Ss 304 H, *Adv Mater Process Technol*, 2023; 1–25.
- Li X., Nie J., Wang X., Li K., and Zhang H. Failure analysis of dissimilar metal welds between ferritic heat resistant steels and austenitic stainless steels in power plant, *Chinese J. Mech. Eng.*, 2024; 37(1): 76.
- Al Hajri M., Malik A. U., Meroufel A., and Al-Muaili F. Premature failure of dissimilar metal weld joint at intermediate temperature superheater tube, *Case Stud. Eng. Fail. Anal.*, 2015; 3: 96–103. <https://doi:10.1016/j.csefa.2015.03.006>
- A. I., S. Institute. *Welding of Stainless Steels and Other Joining Methods - A Designers' Handbook Series*. 1988; 6: 11.
- Gandy D. *The Grades 11 and 12 Low Alloy Steel Handbook 1¼Cr½Mo, 1Cr½Mo, 13CrMo44*. 2007; 3(3). Available from: www.epri.com
- Avery RE. *Guidelines for welding dissimilar metals*. Am Inst Chem Eng. 1991; May.
- Shravan C., Radhika N., Deepak Kumar N. H., and Sivasailam B. A review on welding techniques: properties, characterisations and engineering applications, *Adv. Mater. Process. Technol.*, 2023; 10(2): 1126–1181. <https://doi:10.1080/2374068X.2023.2186638>
- Rathod D. W., Pandey S., Singh P. K., and Prasad R. Mechanical properties variations and comparative analysis of dissimilar metal pipe welds in pressure vessel system of nuclear plants, *J. Press. Vessel Technol.*, 2016; 138(1): 11403. <https://doi:10.1115/1.4031129>
- Chen Z. R., Lu Y. H., Ding X. F., and Shoji T. Microstructural and hardness investigations on a dissimilar metal weld between low alloy steel and Alloy 82 weld metal, *Mater. Charact.*, 2016; 121: 166–174. <https://doi:10.1016/j.matchar.2016.09.033>
- Handbook M. *Welding, brazing, and soldering*. 1993; 6: 322.
- Sharma P. and Dwivedi D. K. Enhancing mechanical properties of dissimilar steel A-TIG weld joint by in-situ induction post-heating, *Manuf. Lett*. 2024; 42: 30–3.
- Chuaiphan W. and Srijaorenpramong L. Optimization of gas tungsten arc welding parameters for the dissimilar welding between AISI 304 and AISI 201 stainless steels, *Def. Technol.*, 2019; 15(2): 170–178, <https://doi:10.1016/j.dt.2018.06.007>
- Afrox. *Afrox Product Reference Manual - Welding Consumables - Stainless Steel*. 2017; 1–21.
- He Y. and Xing Z. Investigations on the microstructure, mechanical properties and corrosion resistance of SUS 304 austenitic stainless steel welded joints by pulsed current gas tungsten arc welding, *Mater. Res. Express*, 2019; 6(8): 88001. <https://doi:10.1088/2053-1591/ab1b85>
- Gupta A., Singh J., and Chhibber R. Dissimilar welding of austenitic and ferritic steels using nickel and stainless-steel filler: Associated issues, *Proc. Inst. Mech. Eng. Part E J. Process Mech. Eng.*, 2024; 238(5): 2524–2544. <https://doi:10.1177/09544089231159776>
- Asadollahi A., Bahrami A., and Shamanian M. The effects of filler metal and butter layer on the microstructure and mechanical properties of API 5L X65/AISI 304L joint, *J. Mater. Res. Technol.*, 2023; 23: 4148–4166. <https://doi:10.1016/j.jmrt.2023.02.063>
- Khan M., Dewan M. W., and Sarkar M. Z. Effects of

- welding technique, filler metal and post-weld heat treatment on stainless steel and mild steel dissimilar welding joint, *J. Manuf. Process.*, 2021; 64: 1307–1321. <https://doi.org/10.1016/j.jmapro.2021.02.058>
21. Sun Y. L. et al. Effects of dilution on alloy content and microstructure in multi-pass steel welds, *J. Mater. Process. Technol.*, 2019; 265: 71–86. <https://doi.org/10.1016/j.jmatprotec.2018.09.037>
 22. Kah P., Shrestha M., and Martikainen J. Trends in joining dissimilar metals by welding, *Appl. Mech. Mater.*, 2014; 440: 269–276. <https://doi.org/10.4028/www.scientific.net/AMM.440.269>
 23. Ramakrishnan P. *Welding Metallurgy*. 1972; 4(3). <https://doi.org/10.22486/iwj.v4i3.150243>
 24. Sonar T. et al. A critical review on dissimilar welding of ferritic-martensitic steel and austenitic stainless steel using gas tungsten arc welding process: Weldability issues, processing, and performance characteristics of joints, *J. Manuf. Process.*, 2025; 133: 811–864. <https://doi.org/10.1016/j.jmapro.2024.11.081>
 25. Alcantar-Modragón N., García-García V., Reyes-Calderón F., Villalobos-Brito J. C., and Vergara-Hernández H. J. Study of cracking susceptibility in similar and dissimilar welds between carbon steel and austenitic stainless steel through finger test and FE numerical model, *Int. J. Adv. Manuf. Technol.*, 2021; 116: 2661–2686. <https://doi.org/10.1007/s00170-021-07596-0>
 26. Lee S. H. A hot cracking on dissimilar metal weld between A106Gr. B and A312 TP316L with buttering ERNiCr-3, *Metals (Basel)*, 2019; 9(5): 533. <https://doi.org/10.3390/met9050533>
 27. Santosh R., Das G., Kumar S., Singh P. K., and Ghosh M. Experimental and computational investigation of structural integrity of dissimilar metal weld between ferritic and austenitic steel, *Metall. Mater. Trans. A*, 2018; 49(6): 2099–2112. <https://doi.org/10.1007/s11661-018-4554-y>
 28. Li S., Li J., Sun G., and Deng D. Modeling of welding residual stress in a dissimilar metal butt-welded joint between P92 ferritic steel and SUS304 austenitic stainless steel, *J. Mater. Res. Technol.*, 2023; 23: 4938–4954.
 29. Singh D. K., Sahoo G., Basu R., Sharma V., and Mohtadi-Bonab M. A. Investigation on the microstructure—mechanical property correlation in dissimilar steel welds of stainless steel SS 304 and medium carbon steel EN 8, *J. Manuf. Process.*, 2018; 36: 281–292. <https://doi.org/10.1016/j.jmapro.2018.10.018>
 30. Osoba L. O., Ekpe I. C., and Elemuren R. A. Analysis of dissimilar welding of austenitic stainless steel to low carbon steel by TIG welding process, 2015; 5(5): 1–12.
 31. Li X. et al. Characterization and formation mechanism of ultra-fine ferrite grains in dissimilar metal weld between austenitic stainless steel and low alloy ferritic steel,” *Mater. Charact.*, 2021; 171: 110777. <https://doi.org/10.1016/j.matchar.2020.110777>
 32. Asadollahi A., Bahrami A., and Shamanian M. The effects of filler metal and butter layer on the microstructure and mechanical properties of API 5L X65/AISI 304L joint, *J. Mater. Res. Technol.*, 2023; 23: 4148–4166. <https://doi.org/10.1016/j.jmrt.2023.02.063>
 33. Asadi P., Alimohammadi S., Kohantorabi O., Fazli A., and Akbari M. Effects of material type, pre-heating and weld pass number on residual stress of welded steel pipes by multi-pass TIG welding (C-Mn, SUS304, SUS316). *Thermal Sci Eng Prog* 2019; 16. <https://doi.org/10.1016/j.tsep.2019.100462>
 34. Arivazhagan N., Singh S., Prakash S., Reddy G. M. Investigation on AISI 304 austenitic stainless steel to AISI 4140 low alloy steel dissimilar joints by gas tungsten arc, electron beam and friction welding. *Mater Des.* 2011; 32(5): 3036–50. <https://doi.org/10.1016/j.matdes.2011.01.037>
 35. Wang J., Lu M. X., Zhang L., Chang W., Xu L. N., Hu L. H. Effect of welding process on the microstructure and properties of dissimilar weld joints between low alloy steel and duplex stainless steel”. *Int J Miner Metall Mater.* 2012; 19(6): 518–24. <https://doi.org/10.1007/s12613-012-0589-z>
 36. Sonar T., Ivanov M., Trofimov E., Tingaev A., and Suleymanova I. A critical review on solid-state welding of high entropy alloys—processing, microstructural characteristics and mechanical properties of joints, *Def. Technol.*, 2024; 34: 78–133.
 37. Skowrońska B., Chmielewski T., Golański D., and Szulc J. Weldability of S700MC steel welded with the hybrid plasma+ MAG method, *Manuf. Rev.*, 2020; 7: 4. <https://doi.org/10.1051/mfreview/2020001>
 38. Rathore S. et al. Advanced ultra super critical power plants: Role of buttering layer, *Int. J. Adv. Manuf. Technol.*, 2024; 134(11): 5021–5064.
 39. David S.A., Goodwin G.M., Braski D.N. Solidification behavior of austenitic stainless steel filler metals. Oak Ridge National Lab. (ORNL), Oak Ridge, TN (United States); 1980.
 40. Guiraldenq P. and Duparc O. H. The genesis of the Schaeffler diagram in the history of stainless steel, *Metall. Res. Technol.*, 2017; 114(6): 613. <https://doi.org/10.1051/metal/2017059>
 41. Giudice F., Missori S., Scolaro C., and Sili A. A review on fusion welding of dissimilar ferritic/austenitic steels: processing and weld zone metallurgy, *J. Manuf. Mater. Process.*, 2024; 8(3): 96. <https://doi.org/10.3390/jmmp8030096>
 42. Ming H., Wang J., and Han E.-H. Comparative study of microstructure and properties of low-alloy-steel/nickel-based-alloy interfaces in dissimilar metal

- weld joints prepared by different GTAW methods, *Mater. Charact.*, 2018; 139: 186–196. <https://doi.org/10.1016/j.matchar.2018.02.044>
43. Lu L., Cai Z., Yang J., Liang Z., Sun Q., and Pan J. Study on key parameters of dilution ratio of the bead deposited by GTAW method for nuclear components, *Metals (Basel)*, 2022; 12(9): 1506, <https://doi.org/10.3390/met12091506>
 44. Mas F., Tassin C., Roch F., Yescas M., Todeschini P., and Bréchet Y. Growth morphologies and primary solidification modes in a dissimilar weld between a low-alloy steel and an austenitic stainless steel, *Metals (Basel)*, 2018; 8(4): 284. <https://doi.org/10.3390/met8040284>
 45. Taban E., Kaluc E., and Aykan T. S. Effect of the purging gas on properties of 304H GTA welds, *Weld. J.*, 2014; 93(4): 124–130.
 46. Westin E. M. and Serrander D. Experience in welding stainless steels for water heater applications, *Weld. World*, 2012; 56(5): 14–28. <https://doi.org/10.1007/BF03321346>
 47. Bensaïd N., Benlamnour M. F., Laksir Y. L. D., Saadi T., and Badji R. Optimization of tungsten inert gas welding process parameters for joining austenitic stainless steel and copper using the Taguchi method, *Adv. Sci. Technol. Res. J.*, 2025; 19(1): 209–219. <https://doi.org/10.12913/22998624/195449>
 48. Gajjar P. K., Khatri B. C., and Jha R. Investigation of effect of post weld heat treatment on microhardness and microstructure of auto TIG welded stabilized SA213 TP347H weldments, *Weld. Int.*, 2024; 38(5): 366–382.
 49. Kutelu B. J., Seidu S. O., Eghabor G. I., and Ibi-toye A. I. Review of GTAW welding parameters, *J. Miner. Mater. Charact. Eng.*, 2018; 6(5): 541.
 50. Okonkwo O., Ming H., Wang J., Meng F., Xu X. and Han E.-H. Microstructural characterization of low alloy steel A508–309/308L stainless steel dissimilar weld metals, *Int. J. Press. Vessel. Pip.*, 2021; 190: 104297. <https://doi.org/10.1016/j.ijpvp.2020.104297>
 51. Thakare J. G., Pandey C., Mahapatra M. M., and Mulik R. S. An assessment for mechanical and microstructure behavior of dissimilar material welded joint between nuclear grade martensitic P91 and austenitic SS304 L steel, *J. Manuf. Process.*, 2019; 48: 249–259. *J Manuf Process.* 2019; 48(September): 249–59. <https://doi.org/10.1016/j.jmapro.2019.10.002>
 52. Skowrońska B., Chmielewski T., and Zasada D. Assessment of selected structural properties of high-speed friction welded joints made of unalloyed structural steel, *Materials (Basel)*, 2022; 16(1): 93. <https://doi.org/10.3390/ma16010093>
 53. Azwinur M.H, Usman K., Dharma S., and Akhyar. Effects of heat input on mechanical properties, microstructures and thermal conductivity of copper alloy in gas tungsten arc welding technology. *Adv. Sci. Technol. Res. J.*, 2025; 19(6): 316–329. <https://doi.org/10.12913/22998624/203367>